NASA Contractor Report 4454

Probability Density Functions in Turbulent Channel Flow

Surya P. G. Dinavahi
Analytical Services & Materials, Inc.
Hampton, Virginia

Prepared for
Langley Research Center
under Contract NAS1-18599

National Aeronautics a
Space Administration
Office of Management
Scientific and Technic
Information Program

1992

(NASA-CR-4454) PROBABILITY DENSITY FUNCTIONS IN TURBULENT CHANNEL FLOW (Analytical Services and Materials) 23 p

N93-12399

Unclas

H1/02 0127094

481117

Probability Density Functions in Turbulent Channel Flow

Surya Prasad G. Dinavahi
A S & M Inc.

Abstract

The probability density functions (pdf's) of the fluctuating velocity components, as well as their first and second derivatives, are calculated using data from the direct numerical simulations (DNS) of fully developed turbulent channel flow. It is observed that, beyond the buffer region, the pdf of each of these quantities is independent of the distance from the channel wall. It is further observed that, beyond the buffer region, the pdf's for all the first derivatives collapse onto a single universal curve and those of the second derivatives also collapse onto another universal curve, irrespective of the distance from the wall. The kinetic-energy dissipation rate exhibits log normal behaviour.

1 Introduction

It has long been known that the probability density functions (pdf's) of the velocity fluctuations in isotropic turbulence are Gaussian, whereas those of the velocity derivatives deviate significantly from Gaussian. This behaviour in grid generated turbulence was first observed experimentally by Batchelor and Townsend (1949), and later on by Kuo and Corrsin (1971). This fact was later confirmed by She, Jackson and Orszag (1988) using the data from direct numerical simulations of isotropic turbulence. The first derivatives of the velocities are observed to have exponential tails, Narasimha (1989). However, the dissipation rate of kinetic energy, which is the sum of squares of the velocity derivatives in different directions, is known to exhibit log normal behaviour. This was verified experimentally by Kuo and Corrsin (1971) and by several other investigators referred in their work.

The presence of exponential tails in the pdf's of the derivatives implies greater intermittency in the small scale structures. The fact that, even though the pdf's of the velocities are

close to Gaussian, the derivative pdf's have exponential tails, implies that the behaviour of the small scale structures is not influenced significantly by the presence of the larger scale structures. The knowledge about the pdf of dissipation rate gives us a better picture about the intermittency of small scales and may help in developing or assessing the turbulence models. The modeled moments for the dissipation rate can be compared with those of the log normal pdf. Ascertaining the shapes of the pdf's of the velocities and their derivatives is expected, at a later stage, to help in the development and assessment of the stochastic turbulence models.

The aim of the present work is to observe the nature of the probability distributions of the velocity fluctuations, their derivatives and the energy dissipation rate in wall-bounded turbulence. In particular, we would like to examine whether the pdf's depend on the distance from the wall or whether they are universal with respect to the wall normal direction. Such a universality of the pdf's was shown by Balachandar and Sirovich (1991) in Rayleigh-Benard convection problem.

In Section 2, a brief description of the DNS data, the coordinate system and the pdf's is given. In Section 3, the question of independence with respect to wall normal direction of the velocity pdf's is examined. In Section 4, the pdf's of the first derivatives of the velocities are examined. In particular the pdf's are examined for independence of wall normal direction and the behaviour of the tails. In Section 5, the second derivatives are examined for independence in the wall normal direction. In Section 6, the log normality of the dissipation rate is examined. We conclude with a brief summary in Section 7.

2 Preliminary Considerations

In our discussions we follow the conventional coordinate system in which x is the streamwise direction, y is the wall normal direction and z is the spanwise direction. We will also use the indices 1, 2 and 3 to denote x, y and z directions, respectively, and a comma (,) followed by a subscript denotes a derivative with respect to the subscript.

The data used in this study are from *temporal* DNS of turbulent incompressible channel flow. In temporal simulations the flow is assumed to be periodic in the streamwise and spanwise directions and to evolve in time. Hence the streamwise and spanwise directions are the homogeneous directions. The DNS data of Zang at a Reynolds number of 318 based on the channel half height and the wall friction velocity, used in Dinavahi and Zang (1991), are used in the present study. Five y locations are selected for pdf calculations. They are selected so as to get one point in the viscous sublayer ($y < y_s$), one in the buffer region between the sublayer and the log layer ($y < y_s$), two in the log layer, and one on the center line. The y locations can be selected easily from a plot of u^+ vs y^+ and are shown as symbols in Figure 1, where $u^+ = u/u_\tau$, $y^+ = yu_\tau/\nu$ and u_τ, and ν are the wall friction velocity and kinematic viscosity, respectively. The value of y_s is such that for any $y > y_s$ the point is outside the viscous sublayer and the buffer region (see Fig. 1). The y^+ values in the increasing order are: 3.84, 10.12, 63.32, 100.40, and 318.0. By symmetry each selected y corresponds to two horizontal planes: one measured from the bottom plate and one from the top plate, thus doubling the number of points. There are 216 points in the streamwise direction, 108 points in the spanwise direction and 162 points in the wall normal direction. Spanwise symmetry is exploited in these calculations. Twenty realizations from the fully turbulent region are used in the present calculations. We thus have a total of 20 x (2 x 216 x 108) = 933,120 points at a given y location to calculate pdf's. These are close to a million points and are more than sufficient to give well resolved pdf's.

In order to verify the conclusions arrived at by using the above data, the DNS data of Kim (1989) at a Reynolds number of 395 are also used. There are 256 and 192 points in the streamwise and spanwise directions, respectively, and 192 points in the wall normal direction. No symmetry in the spanwise direction is used in these calculations. Only one realization is used in our study and so there are 2 x 256 x 192 = 98,304 points at each y location. The following y^+ locations are selected: 6.24, 20.50, 122.21, 204.17, 386.24. These locations are shown in Figure 2 as symbols.

The pdf's are normalized by the local mean and standard deviation at a given y location. In the current simulations, x and z being the homogeneous directions, the pdf of a random variable ϕ is only a function of the wall normal direction and the Reynolds number of the flow; hence, it can be denoted as $f_\phi(\hat{\phi}; y, R_e)$, where ϕ is the random variable in the physical space, $\hat{\phi}$ is the corresponding sample space variable, and R_e is the Reynolds number of the flow under consideration. This indicates the dependence of pdf on the physical space variable y and the parameter R_e.

3 Velocities

In this section, the pdf's of the fluctuating velocities are examined as a function of the wall normal distance. In all the pdf plots the Gaussian curve has also been plotted as a reference for comparison with the calculated pdf's and the abscissa ψ is the random variable normalized by the local mean and standard deviation. In Figure 3 the pdf's of the u velocity, $f_u(\hat{u}; y, R_e = 318)$, are plotted for three y-locations outside the viscous sublayer. This plot shows that the pdf for the u velocity is independent of the y location. These pdf's are slightly skewed to the left. This implies that at a given Reynolds number a single pdf $f_u(\hat{u}; R_e)$ may be constructed for points outside the buffer region. From Figures 4 and 5 we come to the conclusion that the pdf's for v and w, $f_v(\hat{v})$ and $f_w(\hat{w})$, are also independent of y location (for $y > y_s$).

The pdf's of u, v and w for Reynolds number 395 are plotted in Figures 6, 7 and 8, respectively, and it can be seen that these pdf's are also independent of y.

Hence, it seems that the pdf's of u, v and w, for the two Reynolds numbers considered, are independent of y ($y > y_s$) locations beyond the buffer region, i.e., $f_{u_i}(\hat{u_i}; y, R_e) = f_{u_i}(\hat{u_i})$ for $y > y_s$. Also, the pdfs show only minor deviations from the Gaussian curve, the slight left skewness of the pdf for u being the largest.

4 First Derivatives of the Velocities

In this section, we examine the question of independence of y location for the pdf's of the first derivatives. We will also consider the hypothesis by Narasimha (1989) that the pdf's of the first derivatives are made up of Gaussian core and exponential tails.

In Figure 9, pdf's for $u_{,y}$ at three y locations outside the sub-layer are plotted from the data at a Reynolds number of 318. From this figure it is seen that the pdf's of $u_{,y}$ collapse onto one single curve for $y > y_s$. Similarily, the pdf's of the other first derivatives are also independent of y location. Having established the independence of y location for the first derivatives, pdf's are calculated by using the entire data set from the three y locations for each of the nine derivatives $u_{i,j}$ (i, j=1, 2, 3). These pdf's can be denoted as $f_{u_{i,j}}(\hat{u}_{i,j}; R_e)$, showing the independence of y for $y > y_s$, and are plotted in Figure 10. It can be seen that the pdf's for all nine derivatives fall on the same curve, albeit with some spread in the tails. Upon closer examination, it looks like the nine curves may be divided into two groups depending on their proximity to each other in tails. The quantities, $u_{,x}$, $v_{,y}$, and $w_{,z}$, that go into the continuity equation group together and the other derivatives which go into defining the vorticity components make another group. This will be investigated in more detail in the future.

To see if these observations also hold at another Reynolds number, pdf's for the quantity $v_{,x}$ are plotted in Figure 11, using the data at $R_e = 395$. It can be observed that the pdf's beyond the buffer region collapse onto one curve. Analogous to Figure 10 at R_e=318, pdf's of all the nine first derivatives at R_e=395 are plotted in Figure 12. Figures 10 and 12 suggests that the pdf's of the first derivatives are not only independent of the y location, but also, in fact, all of them even fall onto the same curve at a given Reynolds number.

Having established the independence of y and the universality of the first derivatives, a least squares fit to the function

$$f(x) = ae^{-x^2/\sigma^2} + be^{-\alpha|x|} \tag{1}$$

is determined for the pdf's of all the nine derivatives at each of the two Reynolds numbers. The above shape is that of a Gaussian core and exponential tails, as suggested by Narasimha (1989). The two calculated curves and the experimental data of Van Atta and Chen (1970) are plotted on the same graph in Figure 13. The data of VanAtta and Chen are from an atmospheric boundary-layer experiment conducted at sea level. One can see that the calculations agree quite well with the experiment suggesting that the shape given by equation (1) is a good approximation for the first derivative pdf's.

While still on the subject of the first derivatives, we would like to examine the pdf's $f_{u,_y}(\hat{u},_y ; y, R_e)$ *within* the sublayer. The pdf's at the two y^+ locations *within* the sublayer for both the Reynolds numbers 318 and 395 are plotted in Figure 14. Gaussian pdf is also plotted for reference. It can be seen that $u,_y$ pdf's are quite close to Gaussian within the sublayer.

5 Second Derivatives of the Velocities

We now turn our attention toward the second derivatives of the fluctuating quantities. In Figure 15 the pdf's $f_{u,_{zz}}(\hat{u},_{zz} ; y, R_e = 318)$ are plotted for the three locations beyond the buffer region. It can be seen that all three pdf's fall on the same curve, indicating that the pdf's outside the viscous sublayer are independent of the Reynolds number. Therefore, a single pdf can be calculated by using the data from all of these locations for each of the second derivatives. In Figure 16, the pdf's of the u velocity derivatives $u,_{zx}$, $u,_{zy}$, $u,_{zz}$, $u,_{yx}$, $u,_{yy}$, $u,_{xx}$ are plotted. On the same plot the pdf's of the same second derivatives of v and w are also plotted. These pdf's are so close to each other that they are virtually indistinguishable from each other. This indicates that similar to the first-derivative pdf's, the second derivative pdf's are also independent of the y location and all of them fall on the same curve.

These observations are verified again using the data at $R_e = 395$. The pdf's, $f_{v,_{yx}}(\hat{v},_{yx}; y, R_e)$, of $v,_{yx}$ plotted in Figure 17 show the independence of the y location. The pdf's of the same second derivative quantities as in Figure 16 at R_e=318 are plotted in Figure 18 at R_e=395.

This again shows the independence of the y location and that the pdf's fall on the same curve irrespective of the quantity. Least square fits to the pdf's of the second derivatives at the two Reynolds numbers are plotted in Figure 19 for comparison.

It should be mentioned that in general the pdf's calculated from the data at $R_e = 395$ exhibit a larger spread along the tails. Most likely this is so because of the relatively smaller number (about 100K) of points used in calculating the pdf's from the data at this Reynolds number.

6 Dissipation Rate

In this section, we examine the log normality of the kinetic-energy dissipation rate. The dissipation rate is defined as

$$\epsilon = -\frac{2}{R_e}\overline{u_{i,j}u_{i,j}} \quad (i,j = 1,2,3), \tag{2}$$

where repeated indices imply summation and R_e is the Reynolds number of the flow. In Figures 20 and 21, the pdf's of $log(\epsilon)$ are plotted for $y > y_s$. On the same plot the Gaussian (normal) pdf is plotted for comparison. This clearly demonstrates that at both the Reynolds numbers, the dissipation rate is log normal outside the sublayer and the buffer regions. However, in the sublayer and the buffer region the pdf (not shown) of the logarithm of ϵ is skewed to the left.

7 Concluding Remarks

By analyzing the data at the two Reynolds numbers (318 and 395), it is concluded that the pdf's of the fluctuating quantities are independent of y location when outside the buffer layer. The pdf's of u are skewed slightly to the left. The pdf's of v and w are symmetric and appear to be close to Gaussian.

The pdf's of the first derivatives are independent of y for locations outside the buffer layer. Not only are the derivative pdf's independent of y, but also they appear to have the

same universal shape irrespective of the particular quantity: the shape of a Gaussian core and exponential tails. The fact that the calculated pdf's from a channel flow agree with those from a boundary layer experiment suggests a universality of even more general nature when sufficiently far away from the boundaries. Further, the pdf's of $u_{,y}$ within the viscous sublayer seem to be independent of y location and appear close to Gaussian.

The pdf's of the second derivatives are also independent of y location and, irrespective of the quantity, they all fall on a universal curve. This curve is also made up of a Gaussian core and exponential tails, but it is different from the one for the first derivatives.

The log normality of the dissipation rate for y location outside the viscous sublayer is established at both the Reynolds numbers.

Since all the above conclusions are verified at two different Reynolds numbers, the next question is the Reynolds number independence. This will be examined in a future study. The universality of pdf's in compressible flow will also be investigated.

Acknowledgements

I would like to thank Dr. John Kim for providing the data at Reynolds number of 395 and Dr. Thomas Zang for providing the data at Reynolds number of 318. I appreciate the help provided by Dr. Zang in familiarizing me with his data and DNS programs. I would like to thank Prof. Lawrence Sirovich for fruitful discussions. This work was supported by Theoretical Flow Physics Branch of NASA Langley Research Center under NASA contract number NAS1-18599.

References

[1] Balachandar, S. and Sirovich, L. (1991), 'Probability Distribution Functions in Turbulent Convection,' Phys. Fluids A, Vol. 3, pp. 919-927.

[2] Batchelor, G. K., and Townsend, A. A. (1949), 'The Nature of Turbulent Motion at Large Wave-Numbers,' Proc. R. Soc. London, Ser. A, Vol. 199, pp. 238-255.

[3] Dinavahi, S. P. G., and Zang, T. A. (1991), 'Reynolds Stress Budget in a Transitional Channel Flow,' Proceeding of the ICASE/LaRC Workshop on Transition and Turbulence, July 8 - August 2, 1991.

[4] Kim, J. (1989), 'On the Structure of Pressure Fluctuations in Simulated Turbulent Channel Flow,' NASA TM-101084.

[5] Kuo, A. Y.-S. and Corrsin, S. (1971), 'Expermients on internal intermittency and fine-structure distribution functions in fully turbulent fluid,' J. Fluid Mechanics, Vol. 50, pp. 285-320.

[6] Narasimha, R. (1989), 'The utility and Drawbacks of Traditional Approaches' in Whither Turbulence?, J. L. Lumley (Ed.), pp. 26-28, Springer-Verlag.

[7] She, Z.-S., Jackson, E. and Orszag, S. A. (1988), 'Scale-Dependent Intermittency and Coherence in Turbulence,' J. of Scientific Computing, Vol. 3, No. 4, pp. 407-434.

[8] Van Atta, C. W. and Chen, W. Y. (1970), 'Structure Functions of Turbulence in the Atmospheric Boundary Layer over the Ocean,' J. Fluid Mechanics, vol. 44, pp.145-159.

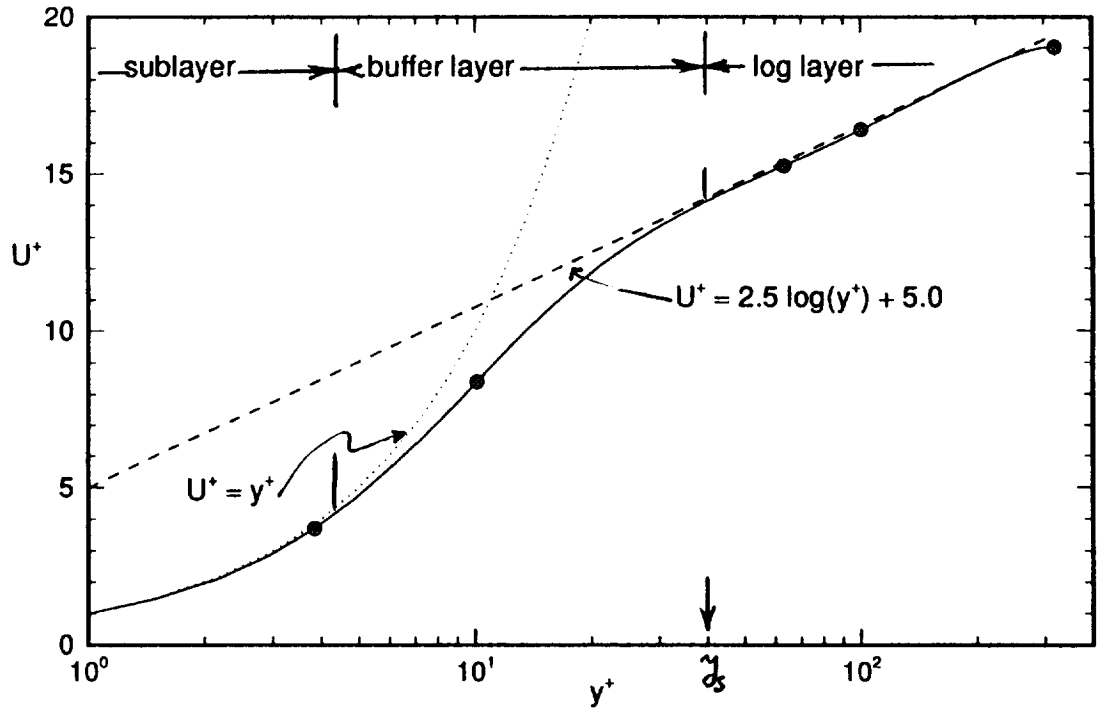


Figure 1. U^+ versus y^+ for Re=318. Symbols represent the y^+ locations at which the pdfs are calculated.

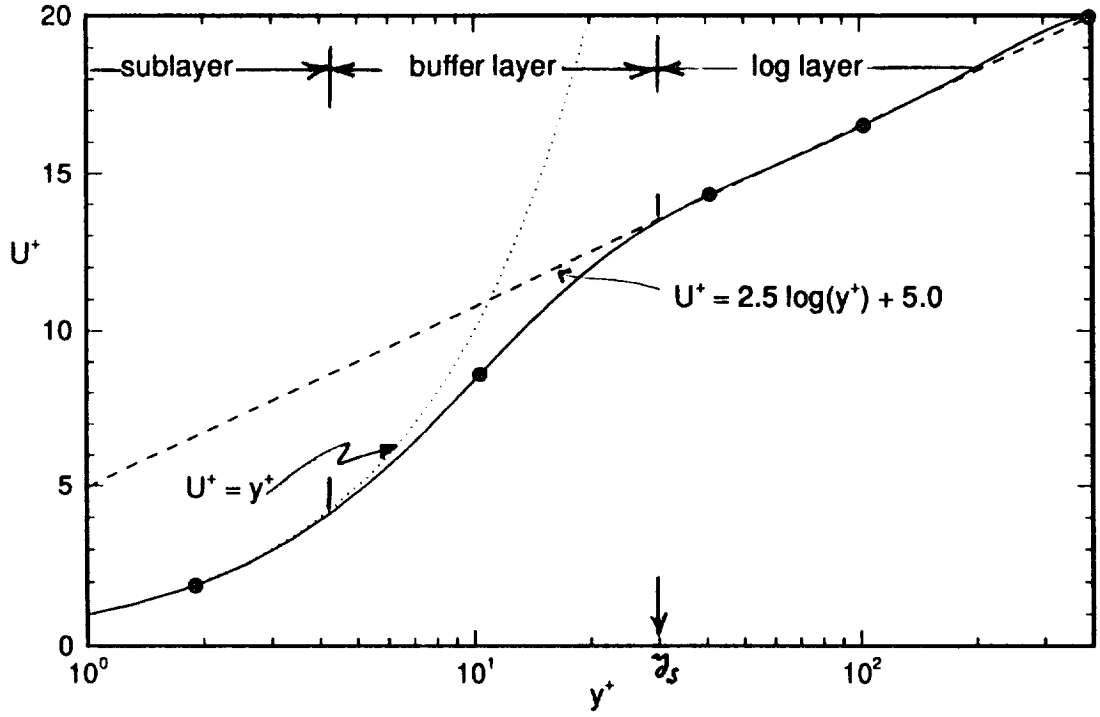


Figure 2. U^+ versus y^+ for Re=395. Symbols represent the y^+ locations at which the pdfs are calculated.

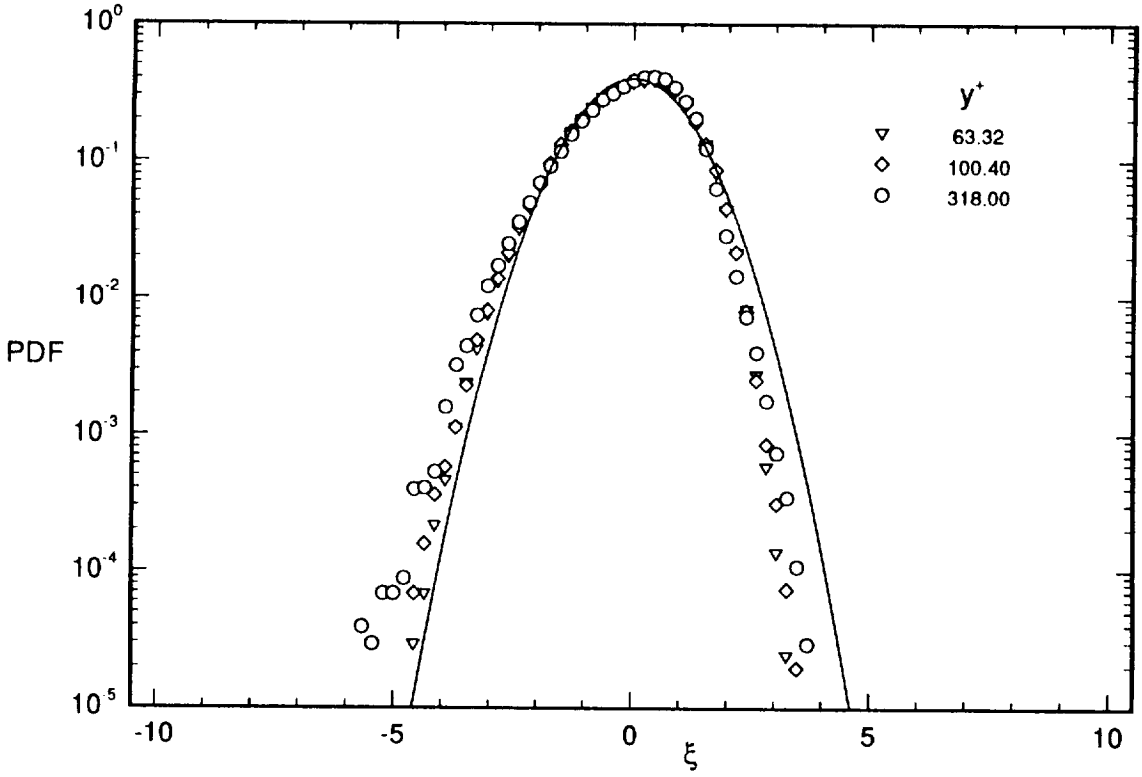


Figure 3. PDFs of u for y beyond the buffer layer for Re=318.
Symbols are from DNS and the solid line is Gaussian.

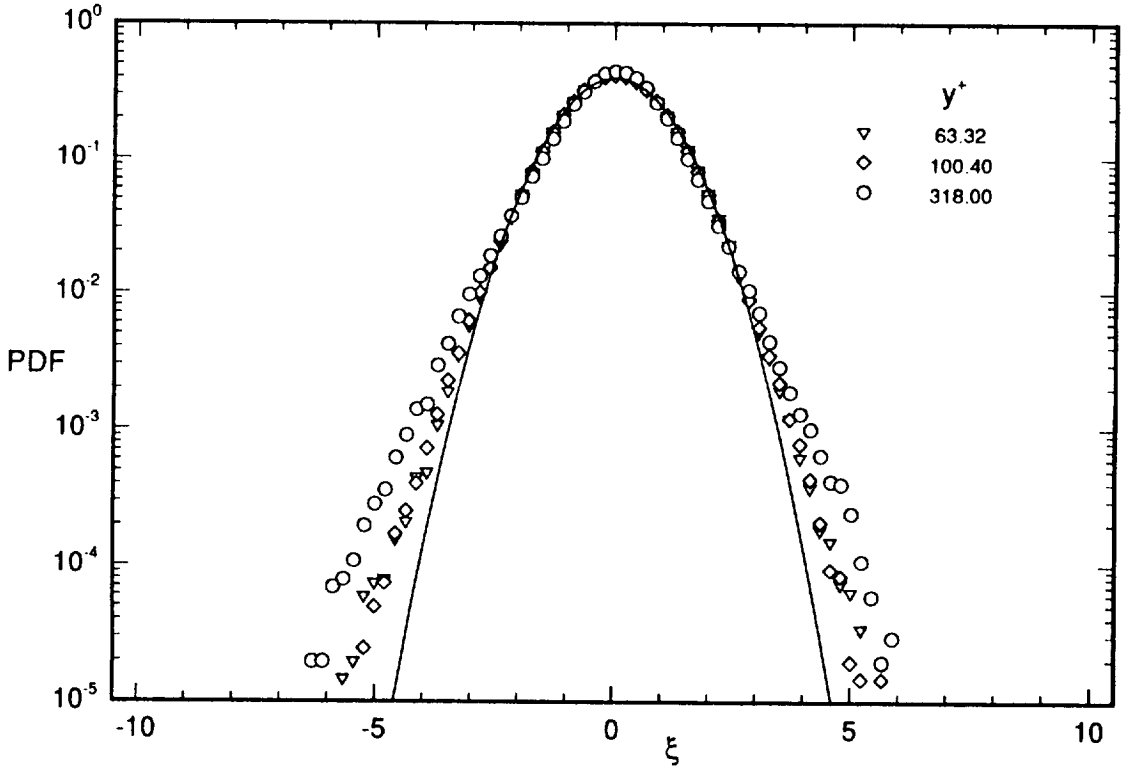


Figure 4. PDFs of v for y beyond the buffer layer for Re=318.
Symbols are from DNS and the solid line is Gaussian.

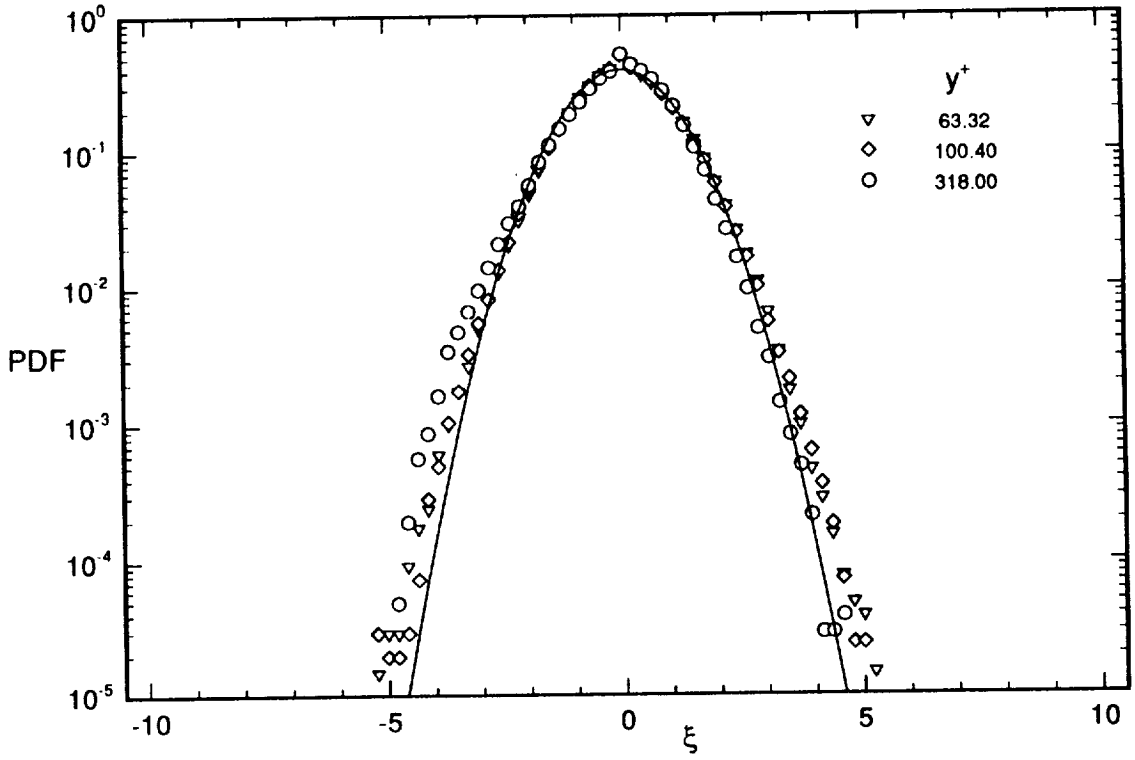


Figure 5. PDFs of w for y beyond the buffer layer for Re=318.
Symbols are from DNS and the solid line is Gaussian.

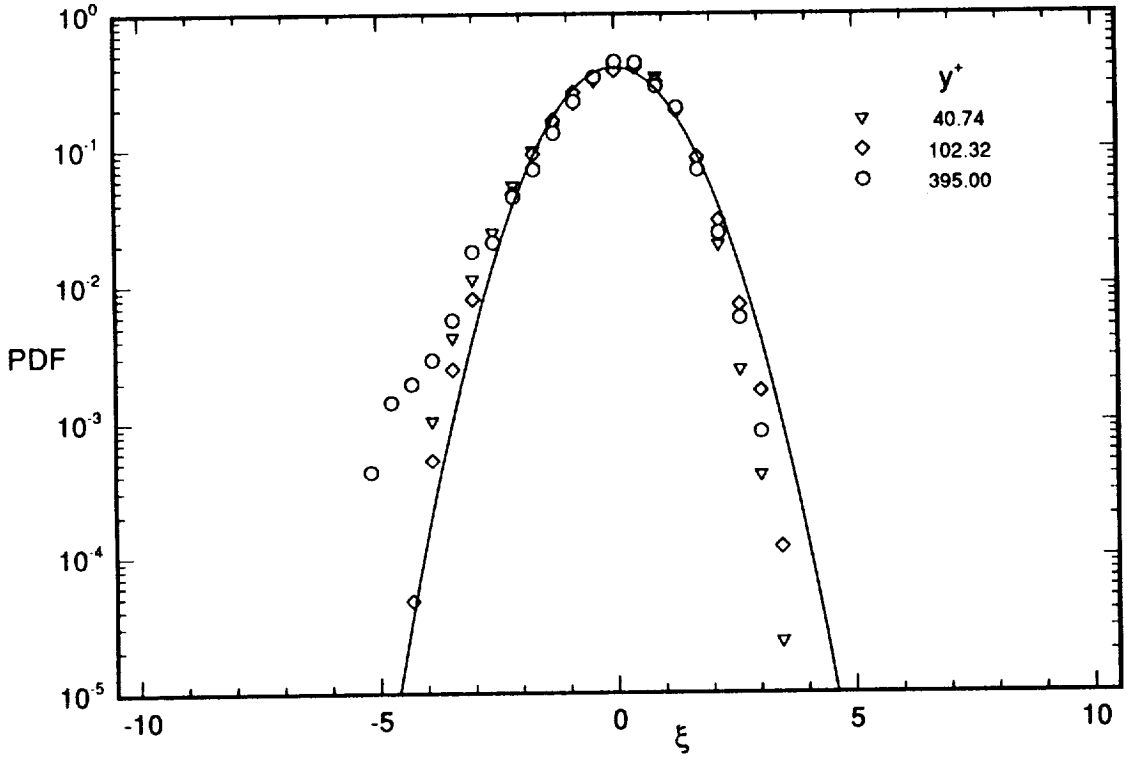


Figure 6. PDFs of u for y beyond the buffer layer for Re=395.
Symbols are from DNS and the solid line is Gaussian.

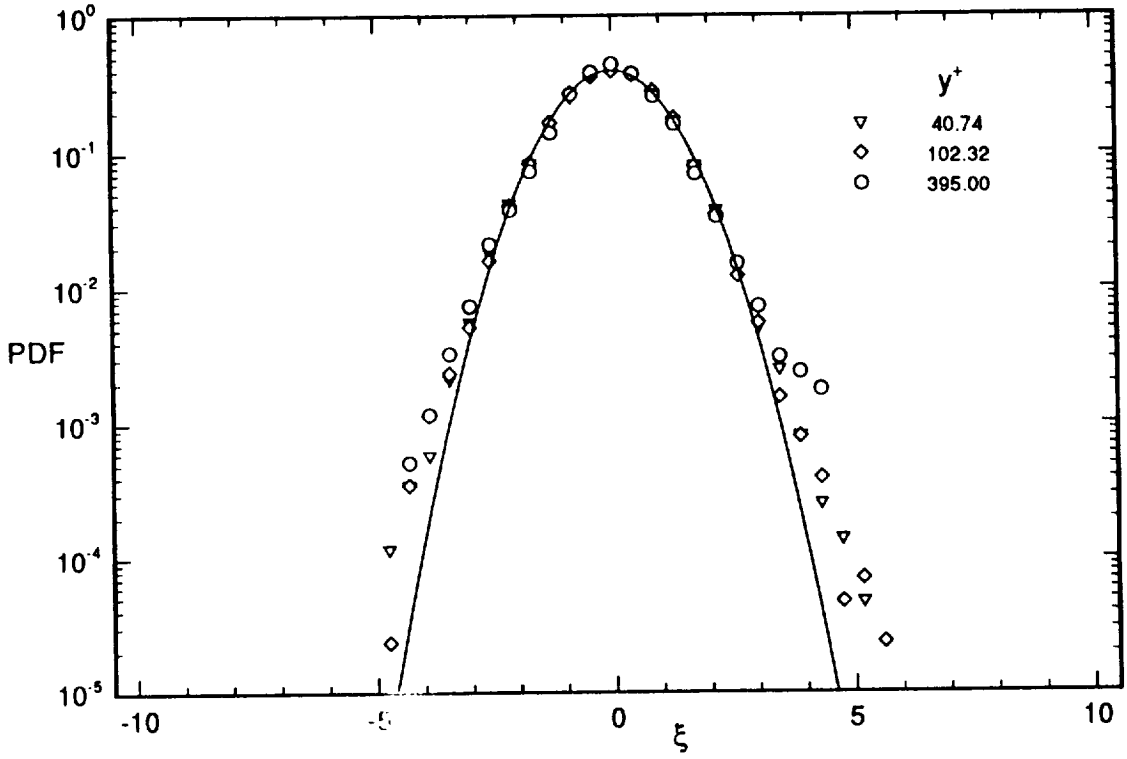


Figure 7. PDFs of v for y beyond the buffer layer for Re=395.
Symbols are from DNS and the solid line is Gaussian.

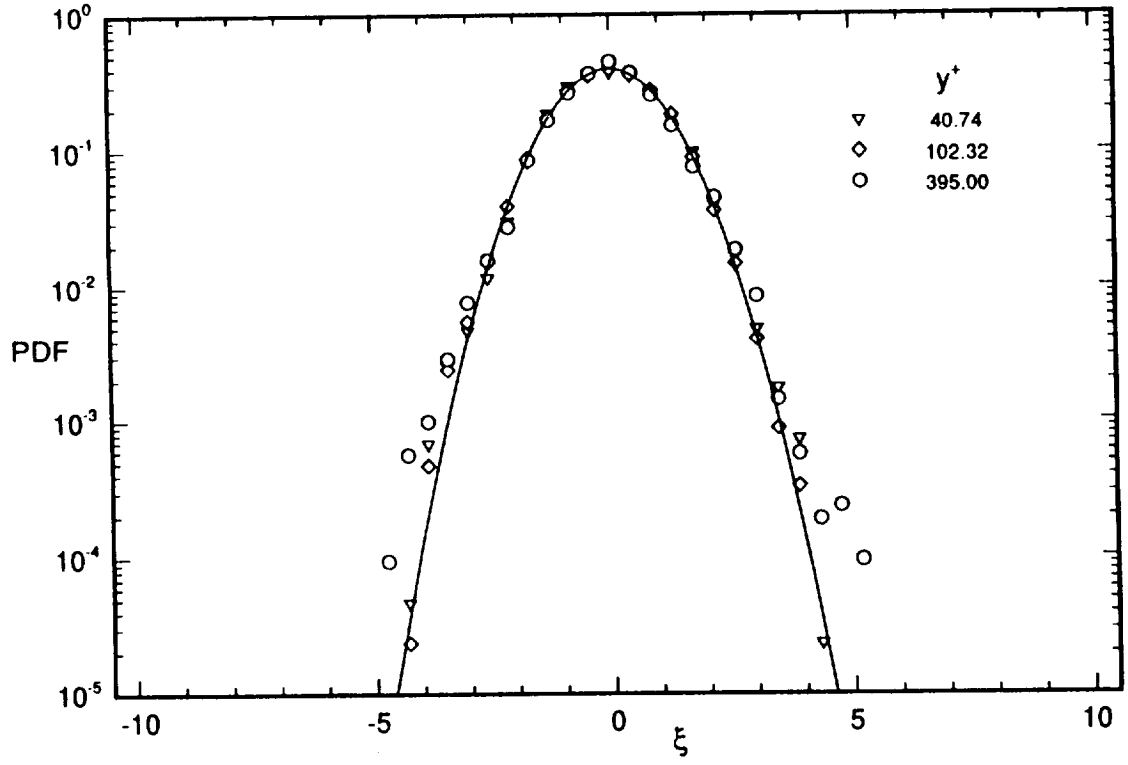


Figure 8. PDFs of w for y beyond the buffer layer for Re=395.
Symbols are from DNS and the solid line is Gaussian.

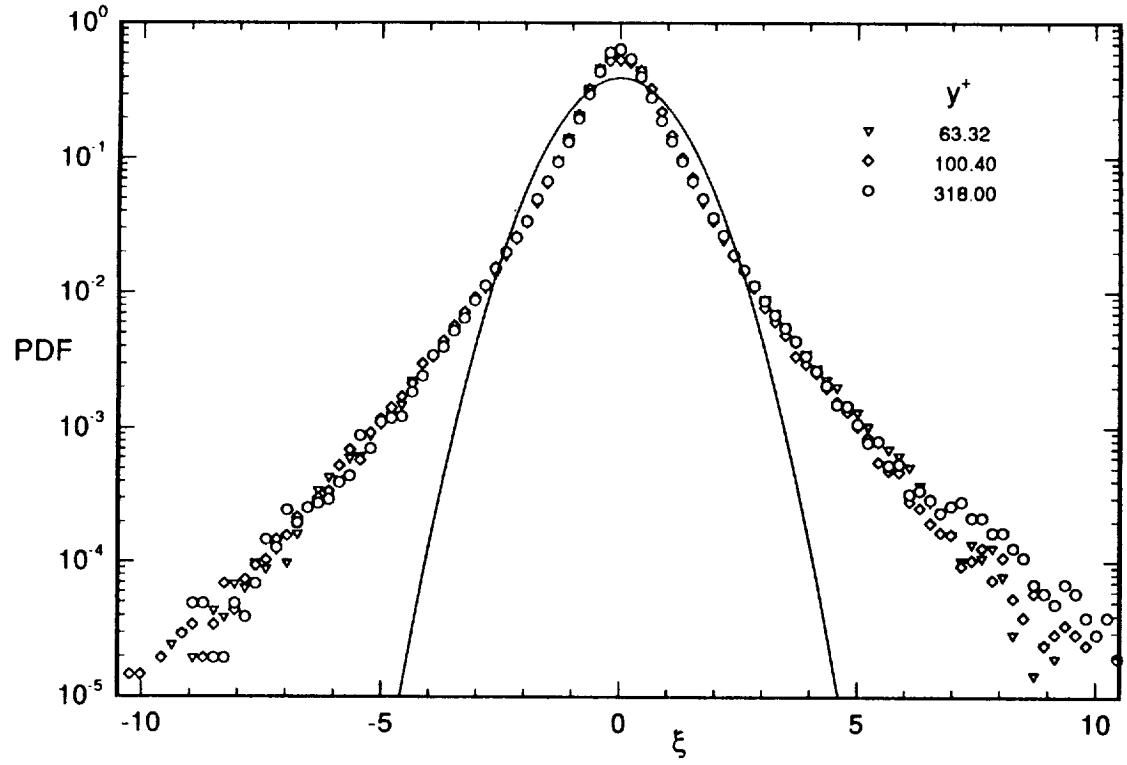


Figure 9. PDFS of $u_{,y}$ for y beyond the buffer layer for Re=318. Symbols are from DNS and the solid line is Gaussian.

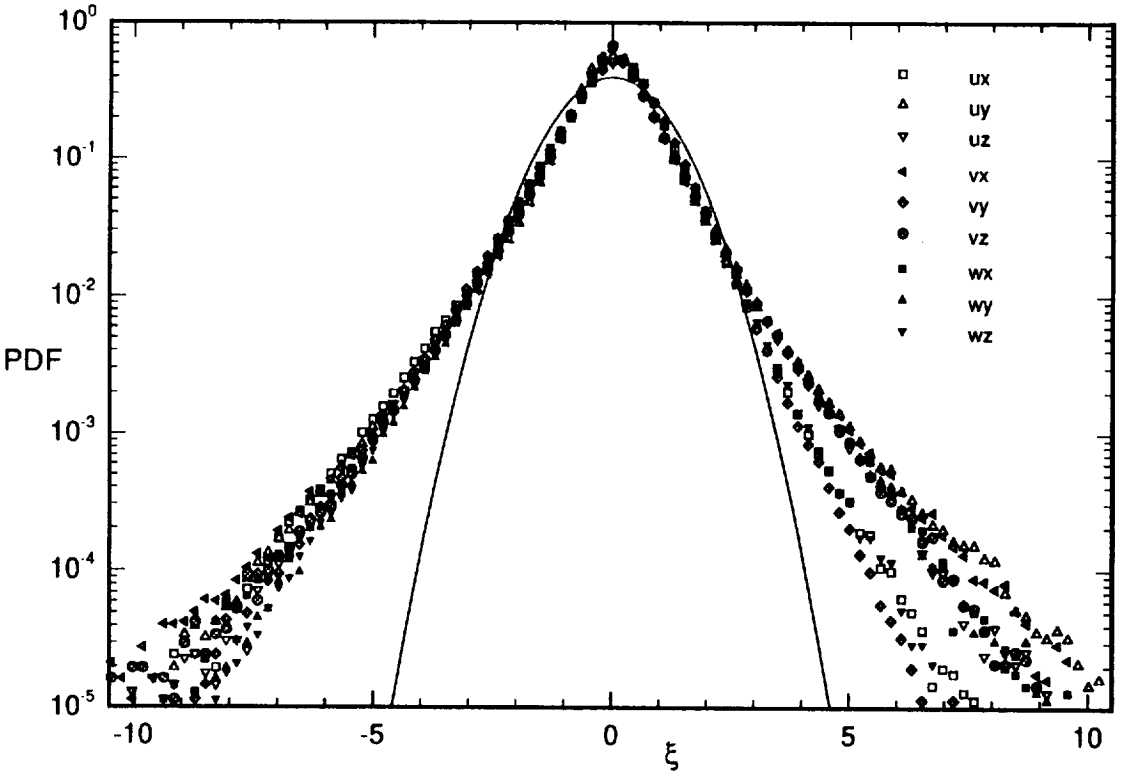


Figure 10. PDFs of the first derivatives for y beyond the viscous sublayer for Re=318. Symbols are from DNS and the solid line is Gaussian.

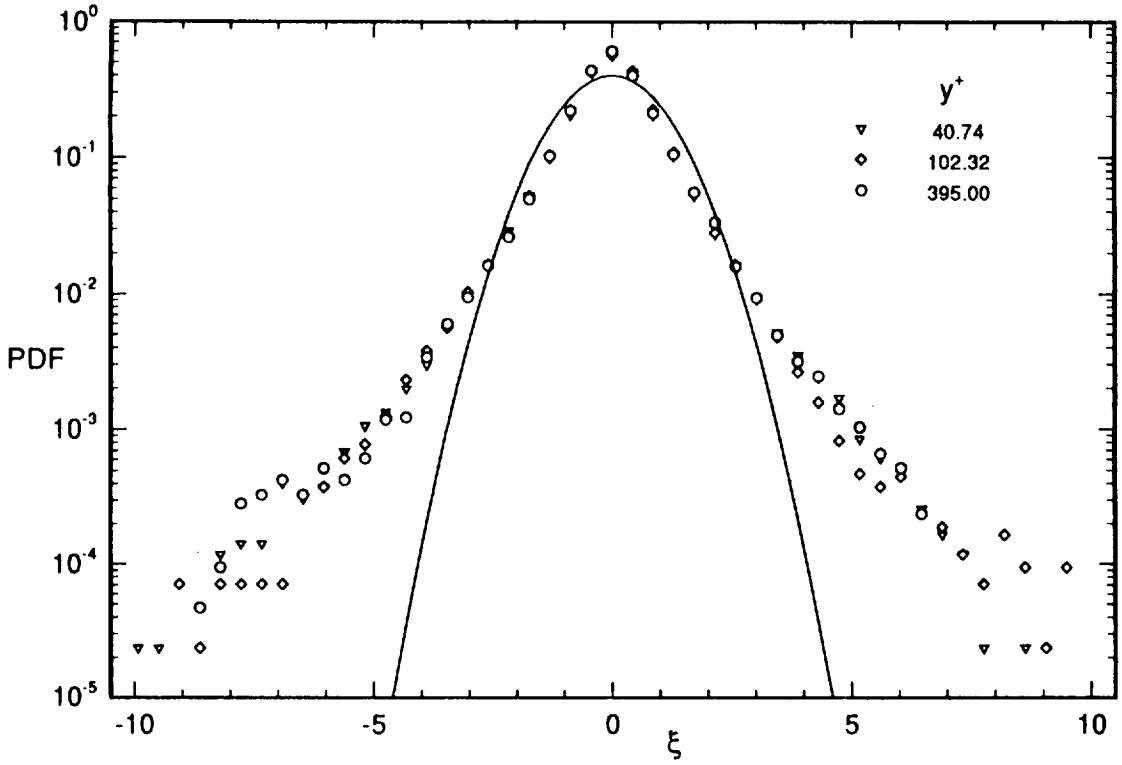


Figure 11. PDFS of $v_{,x}$ for y beyond the buffer layer for Re=395. Symbols are from DNS and the solid line is Gaussian.

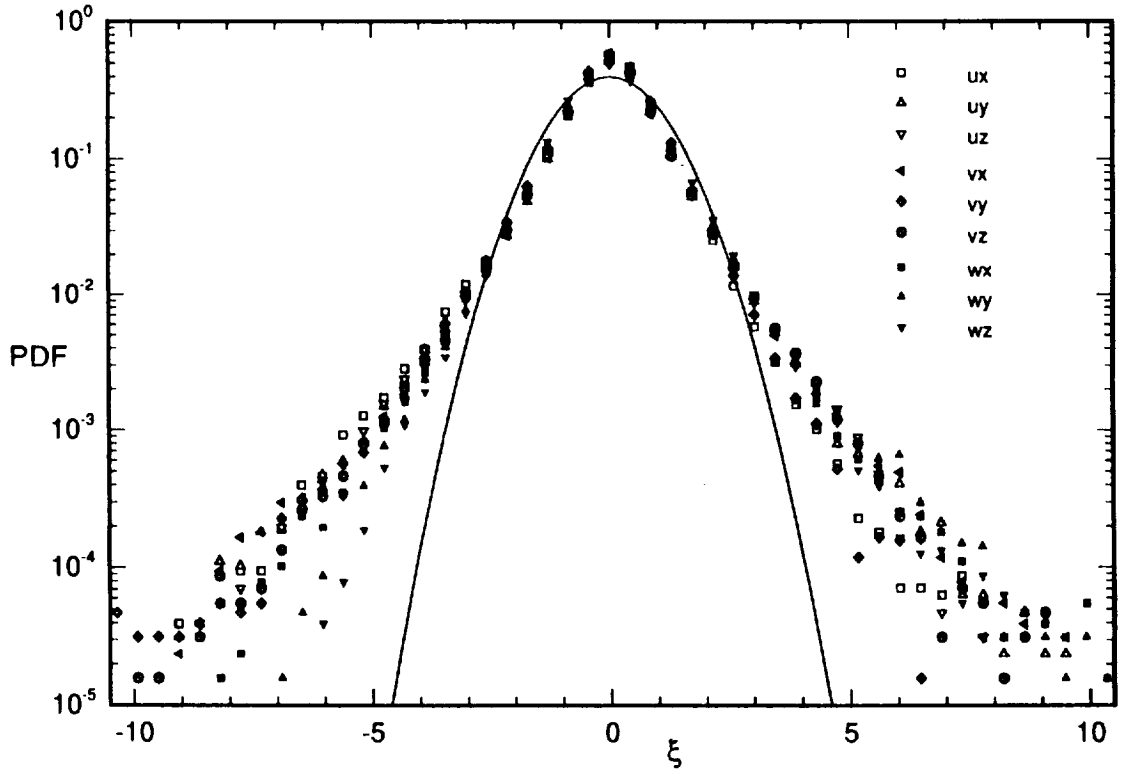


Figure 12. PDFs of the first derivatives for y beyond the viscous sublayer for Re=395. Symbols are from DNS and the solid line is Gaussian.

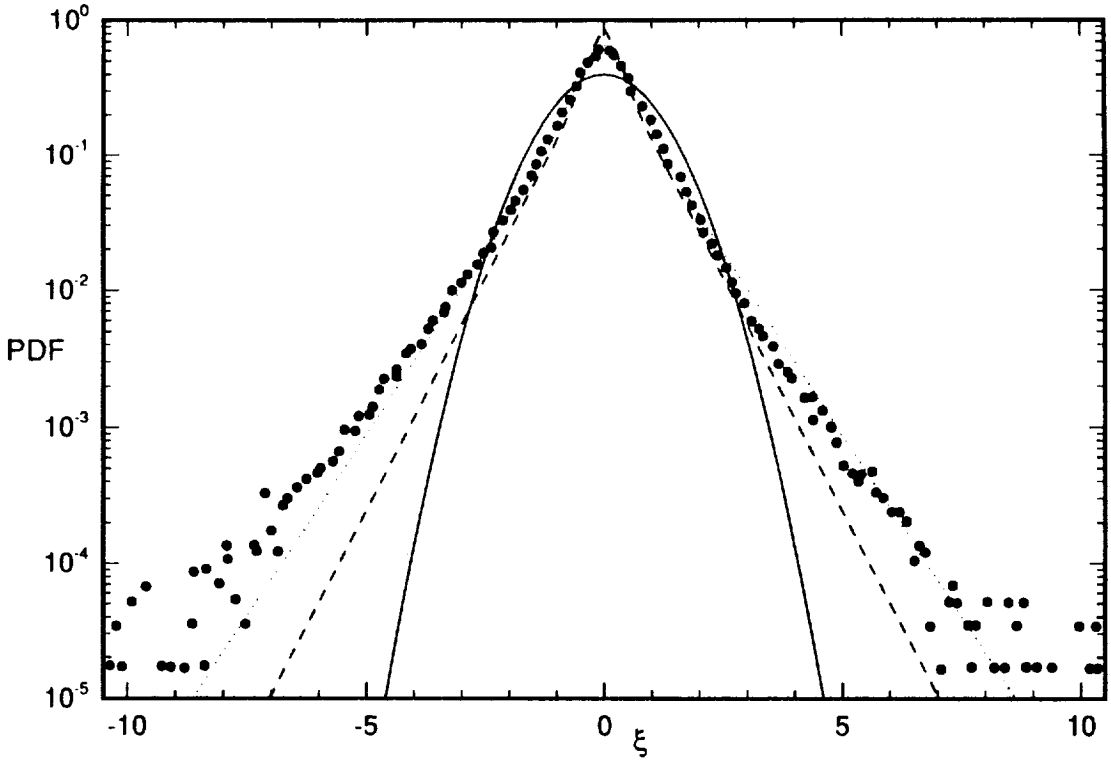


Figure 13. Comparison of DNS data with the experiment of VanAtta and Chen. (--) and (...) are the least squares fits to the pdfs of the first derivatives from the DNS data at Re=318 and 395, respectively. Symbols indicate experiment and the solid line is Gaussian.

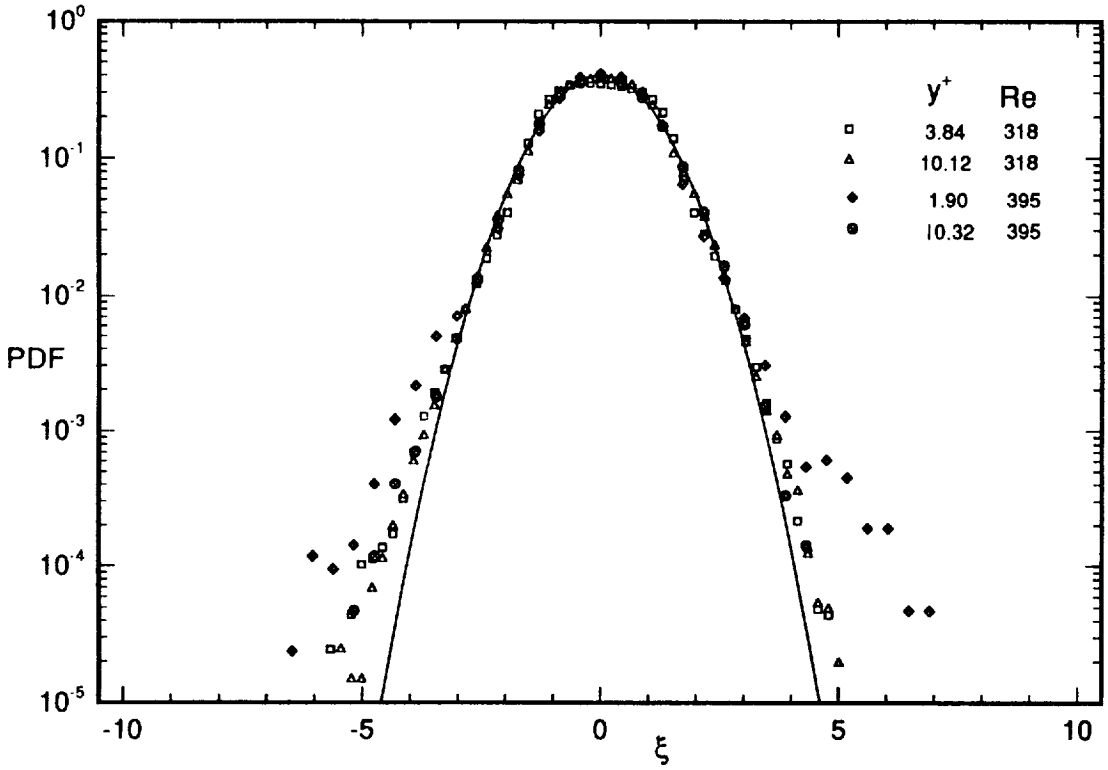


Figure 14. PDFs of $u_{,y}$ for y within the viscous sublayer. Symbols are from the DNS calculations and the solid line is Gaussian.

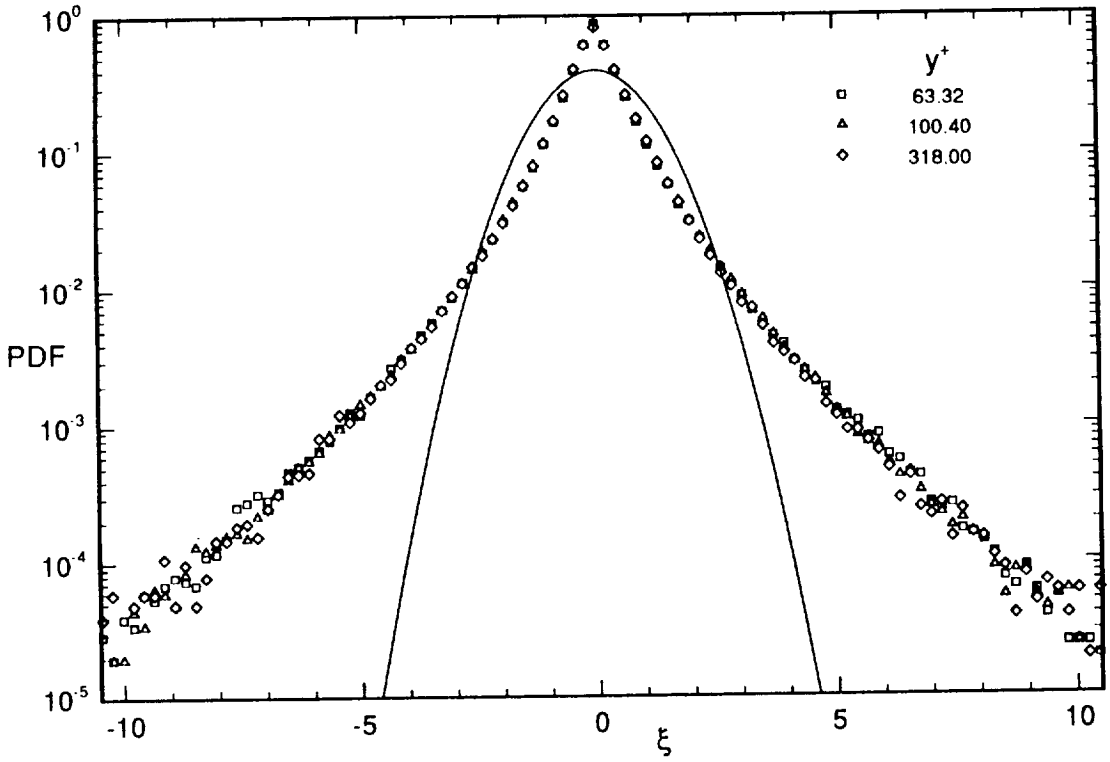


Figure 15. PDFs of $u_{,zx}$ for y beyond the buffer layer for Re=318.
Symbols indicate DNS data and the solid line is Gaussian.

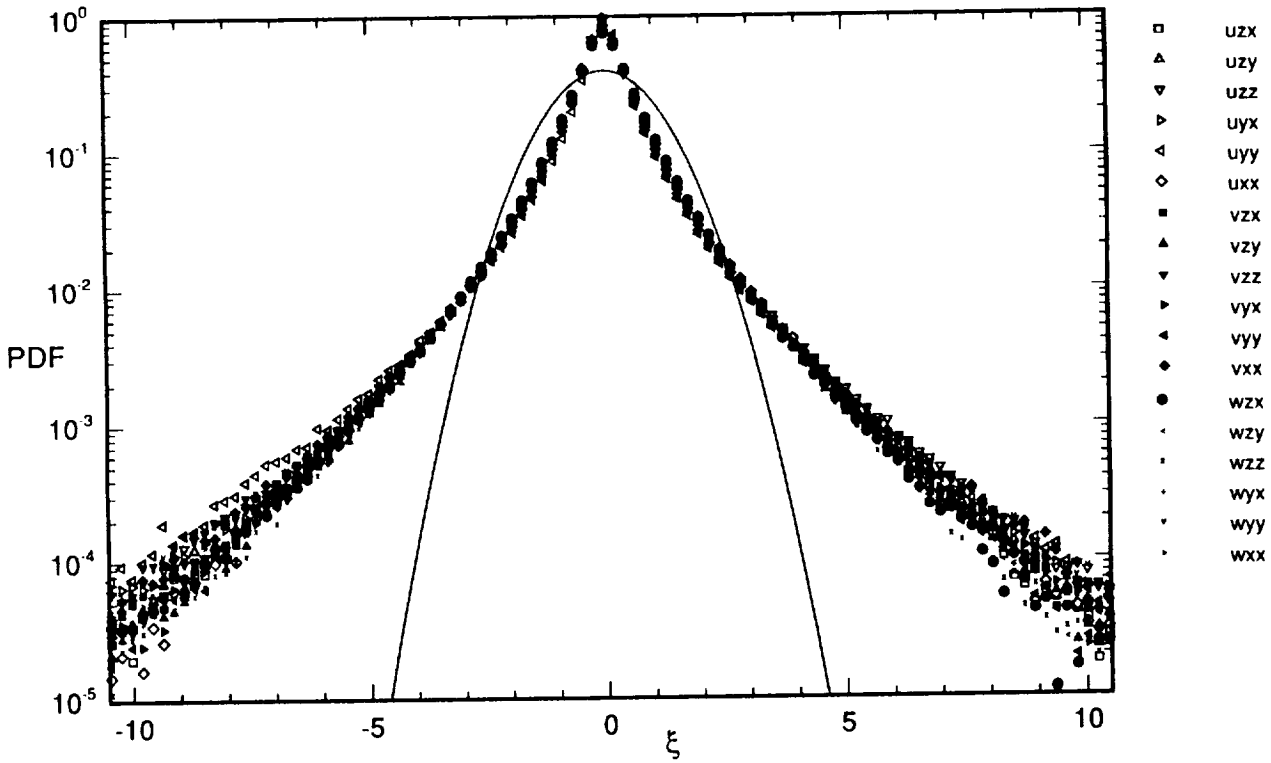


Figure 16. PDFs of the second derivatives for y beyond the buffer layer for Re=318.
Symbols indicate DNS data and the solid line is Gaussian.

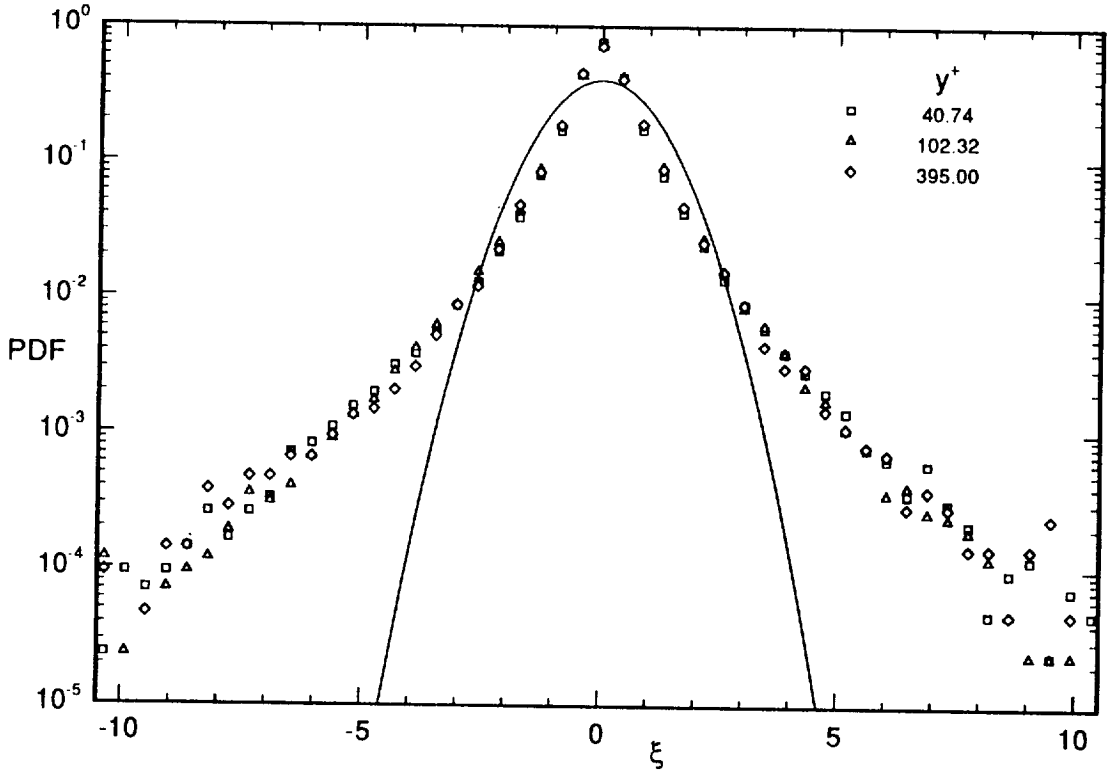


Figure 17. PDFs of $v_{,yx}$ for y beyond the buffer layer for Re=395.
Symbols indicate DNS data and the solid line is Gaussian.

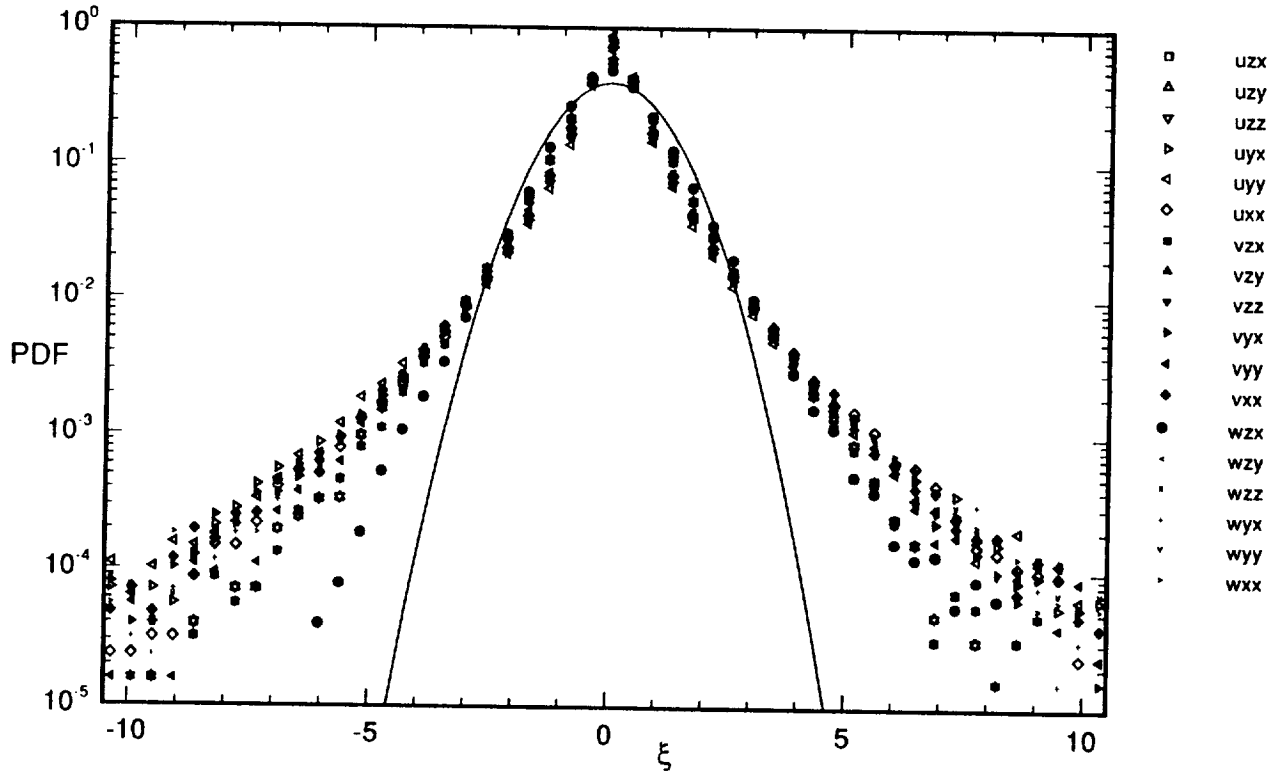


Figure 18. PDFs of the second derivatives for y beyond the buffer layer for Re=395.
Symbols indicate DNS data and the solid line is Gaussian.

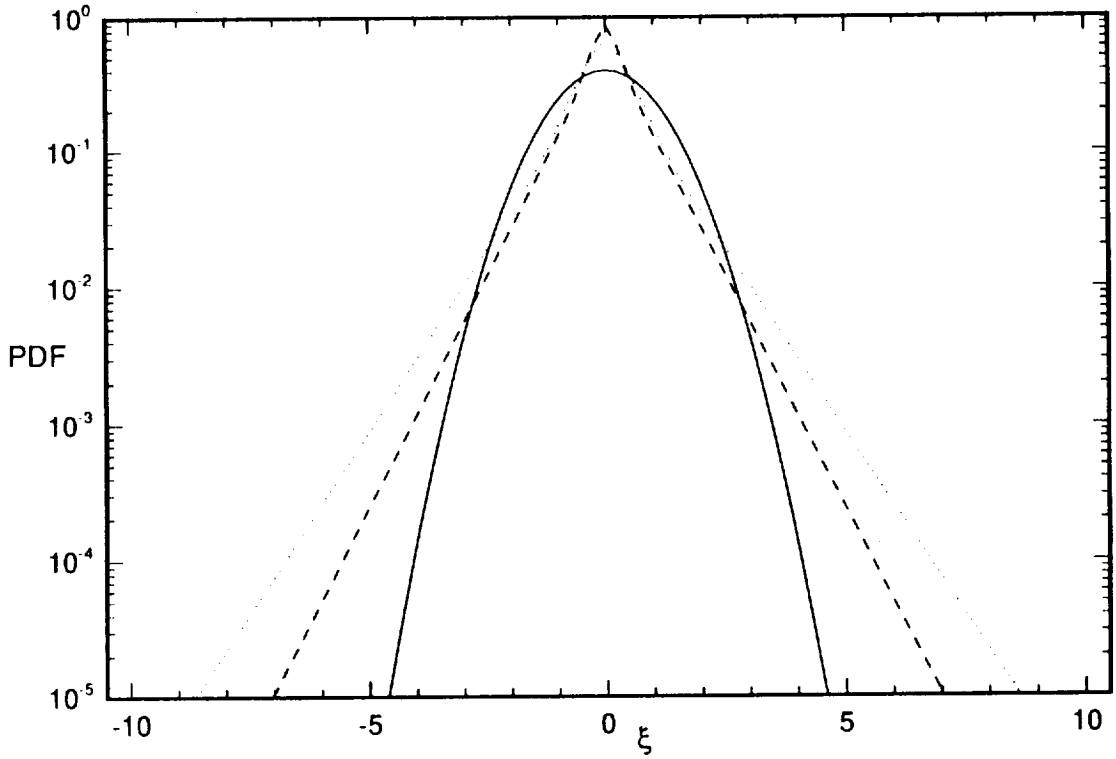


Figure 19. Comparison of least square fits to the pdfs of the second derivatives.
(--) and (...) denote Re=318 and 395, respectively, and the solid line is Gaussian.

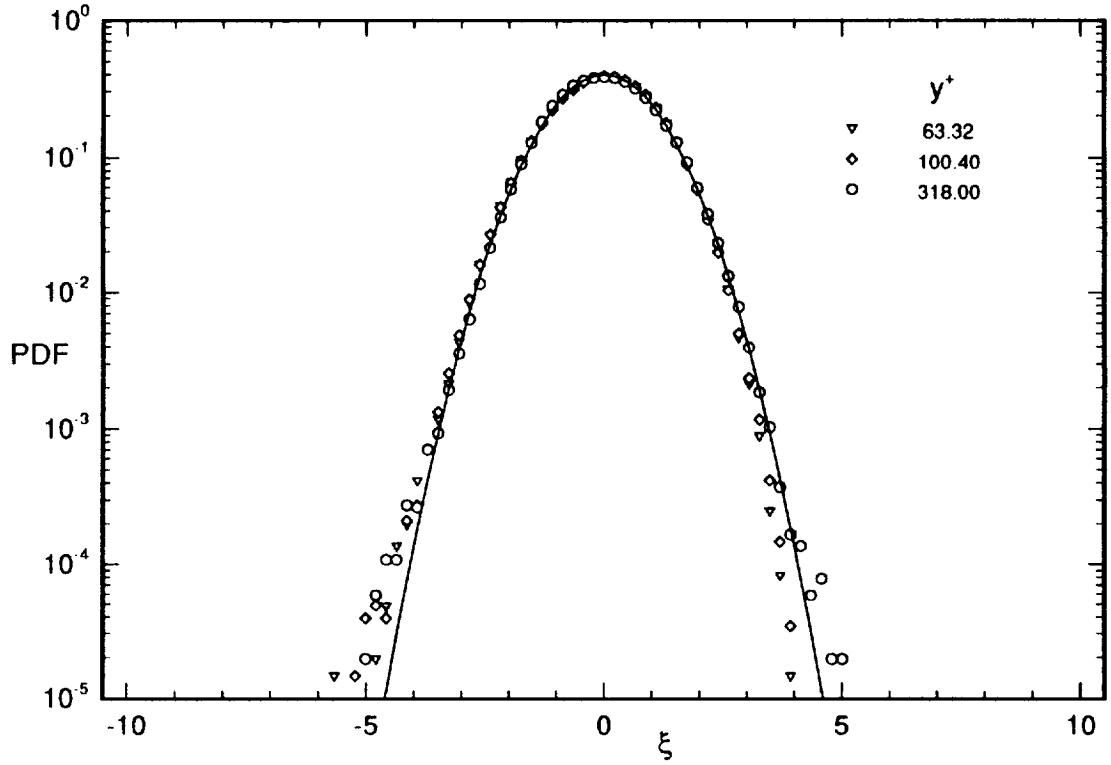


Figure 20. PDFs of log(ε) for Re=318. Symbols are from DNS and the solid line is Gaussian.

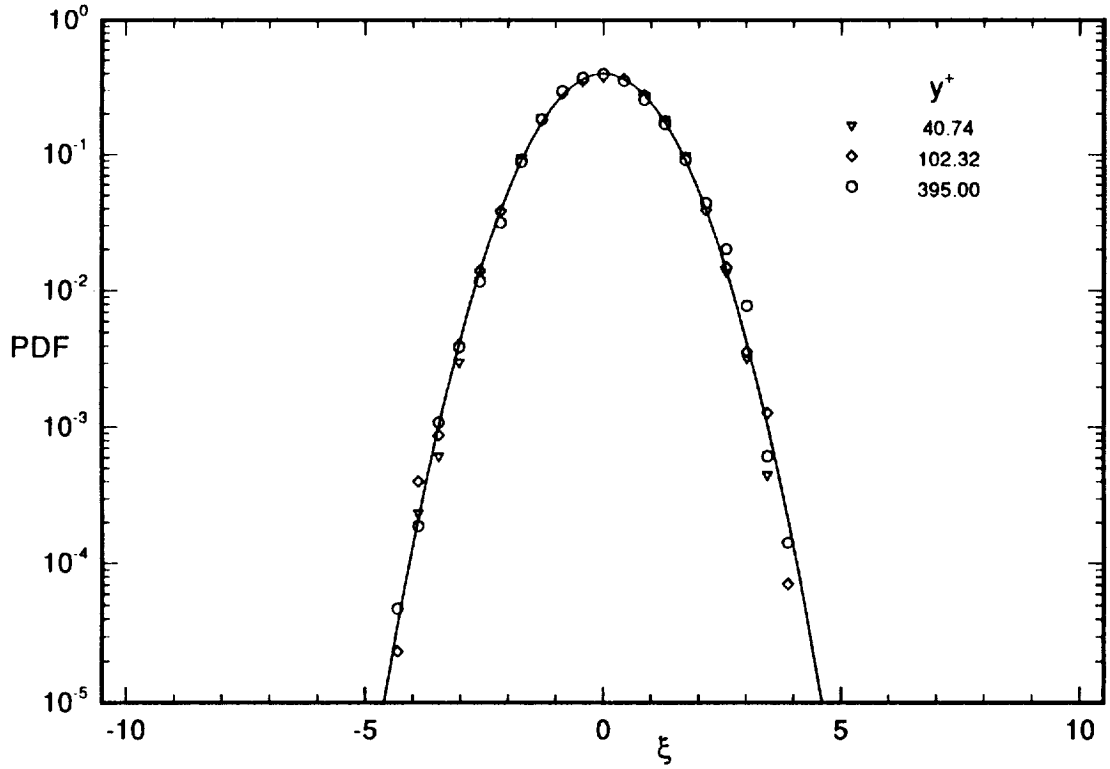


Figure 21. PDFs of log(ε) for Re=395. Symbols are from DNS and the solid line is Gaussian.